Micro PET imaging of ^{18}F-Fluoromisonidazole in an MDA-MB-231 triple negative human breast cancer xenograft model

Zhuzhong Cheng[1,2], Xiao Jiang[2], Li Yang[1], Taipeng Shen[1], Xiaoxiong Wang[2], Hao Lu[2], Jun Wu[1], Chunchao Xia[3], Bin Song[3], Hua Ai[1,3]

[1]National Engineering Research Center for Biomaterials, Sichuan University, Chengdu 610065, China; [2]PET/CT Center, Department of Radiology, Sichuan Cancer Hospital, Chengdu 610041, China; [3]Department of Radiology, West China Hospital, Sichuan University, Chengdu 610041, China

Contributions: (I) Conception and design: Z Cheng, X Jiang, H Ai; (II) Administrative support: J Wu, C Xia, B Song; (III) Provision of study materials or patients: Z Cheng, X Jiang, L Yang, T Shen; (IV) Collection and assembly of data: Z Cheng, X Jiang, H Lu; (V) Data analysis and interpretation: X Wang; (VI) Manuscript writing: All authors; (VII) Final approval of manuscript: All authors.

Correspondence to: Prof. Hua Ai, PhD. National Engineering Research Center for Biomaterials, Sichuan University, Chengdu 610065, China. Email: huaai@scu.edu.cn.

Background: While ^{18}F-Fluoromisonidazole (^{18}F-FMISO) is the most frequently used positron emission tomography (PET) tracer for detecting hypoxia, it has not been studied in a metastatic triple-negative [lack expression of estrogen receptor (ER), progesterone receptor (PR) and human EGF receptor 2 (HER2)] human breast cancer cell xenografts model to our best knowledge. This study focuses on whether ^{18}F-FMISO can detect the hypoxic status of triple-negative human breast cancer (TNBC).

Methods: The TNBC cells MDA-MB-231 were successfully inoculated in right forelimb of nude mice. Nude mice models with TNBC xenografts were assessed by micro-PET imaging with ^{18}F-FMISO, and hypoxic status of the TNBC xenografts was determined by immunohistochemistry. We also compared ^{18}F-FDG uptake, the most commonly used PET tracer in clinical practice, with ^{18}F-FMISO uptake to find out its correlation in MDA-MB-231 xenografts.

Results: For ^{18}F-FMISO, intestines and liver as well as bladder could be seen in micro-PET images. ^{18}F-FDG showed physiologically high uptake in brain, heart, bladder and intestinal tracts. The quantitative radioactivity of ^{18}F-FMISO and ^{18}F-FDG in tumor were 2.18 ± 0.15 and 3.84 ± 0.54 %ID/g, respectively. The quantitative radioactivity of ^{18}F-FMISO and ^{18}F-FDG in muscle were 1.23 ± 0.08 and 0.59 ± 0.09 %ID/g, respectively. The tumor-to-muscle ratios were 1.79 ± 0.015 and 7.11 ± 2.84 for ^{18}F-FMISO and ^{18}F-FDG, respectively. Immunofluorescent images from MDA-MB-231 cryosections showed significant hypoxia.

Conclusions: ^{18}F-FMISO PET may be used for detection of hypoxia in tumor microenvironment of triple negative human breast cancer.

Keywords: ^{18}F-Fluoromisonidazole (^{18}F-FMISO); triple negative breast cancer; micro positron emission tomography (micro PET); hypoxic microenvironment

Introduction

Hypoxia is a pathophysiological property that is defined as a state of depressed oxygen tension. The aberrant growth of tumors exacerbates their susceptibility to hypoxia, especially for malignant solid tumors (1). Since it is well known that hypoxic cancer tissues are more resistant to radiotherapy and chemotherapy than aerobic tissues, tumor hypoxia is often an important determinant of relapse-free survival and overall clinical outcome (2-4). The onset of hypoxia in tumors is associated with and influenced by a sequence of complicated and physiological processes, and could significantly affects the curability of solid tumors, regardless

of treatment modality employed (1). So far, several methods exist to characterize hypoxia directly or indirectly. The polarographic electrode is an invasive, yet direct method for pO_2 measurement, and is often cited as the "gold standard" for hypoxia determination (5). But this method is invasive and can only be used in superficial tumors, does not distinguish between necrotic and viable tissue. Noninvasive imaging of hypoxic cancer cells is of extremely clinical importance for both diagnosis and therapeutic evaluation.

Molecular imaging techniques have therefore become of increasing interest as they are noninvasive and allow repeated 3-dimensional measurements of biological processes *in vivo*. Positron emission tomography (PET) can measure hypoxia using highly specific tracers. Relying on different mechanisms, researchers had developed several kinds of radiotracers, such as ^{18}F-Fluoromisonidazole (^{18}F-FMISO) (6,7), ^{18}F-pentafluorinated etanidazole (^{18}F-EF5) (8,9), ^{18}F-fluoroazomycinarabinofuranoside (^{18}F-FAZA) (10,11), Copper-64 (II) [diacetyl-bis (N4-methylthiosemicarbazone)] (^{64}Cu-ATSM) (12,13). ^{18}F-FMISO has become the predominant PET tracer of these and has been extensively investigated for detecting hypoxia *in vivo* using PET imaging. ^{18}F-FMISO is a radiolabeled analog of the radiosensitizer misonidazole (MISO). Due to its lipophilic character, ^{18}F-FMISO accumulation in hypoxic tumors increases in a period of about 4 hours, while washing out from normoxic tissues starts at 30 min postinjection (14).

While ^{18}F-FMISO is the most frequently used PET tracer for detecting hypoxia, it has not been studied in a metastatic triple-negative [lack expression of estrogen receptor (ER), progesterone receptor (PR) and human EGF receptor 2 (HER2)] human breast cancer cell xenografts model to our best knowledge. The adjuvant treatment of triple-negative human breast cancer (TNBC), which in the absence of any targeted therapy, relied mainly on cytotoxic chemotherapy, such as docetaxel, pirarubicin and cyclophosphamide. Since the hypoxia status of TNBC plays an important role in prognosis of adjuvant chemotherapy, it's important to found out whether ^{18}F-FMISO can describe hypoxic status of tumor microenvironment in TNBC.

In an effort to better characterize ^{18}F-FMISO biodistribution in TNBC models, micro-PET imaging was performed, and hypoxic status of the TNBC tumors was determined by immunohistochemistry. Also, we had compared ^{18}F-FDG uptakes with ^{18}F-FMISO uptakes to find out its correlation in triple negative human breast tumor.

Methods

Cell lines and animals

MDA-MB-231 cell line derived from a metastatic TNBC was purchased from American Type Culture Collection (ATCC, Manassas, VA, USA), and maintained in RPMI-1640 medium (Cellgro, Herndon, VA, USA) supplemented with 10% fetal bovine serum and a mixture of 1% penicilium/streptomycin (Cellgro, Herndon, VA, USA). All experiments with cell lines were conducted within 6 months after obtaining from ATCC. Cell line authentication was done in Sichuan Cancer Hospital (SCCH). The SCCH used short tandem repeat (STR) profiling for characterization and authentication of cell lines. Cells were grown in humidified incubator at 37 °C with 5% carbon dioxide atmosphere. Exponentially growing cells were harvested with 0.25% (w/v) trypsin-0.53 mM EDTA solution, and suspended in phosphate buffer saline.

All animal experimental protocols were conducted in compliance with the guidelines for the care and use of research animals established by the Animals Affairs Committee of Sichuan Cancer Hospital (Permit Number: 20150194). All experiments were performed using 4-wk-old female athymic Balb/c nude mice (weight range, 18–23 g) purchased from SLAC laboratory animal Co., Ltd. The mice were implanted subcutaneously with $1 \times 10^7 / 0.1$ mL MDA-MB-231 cells in the left armpit and were used when the tumors reached approximately 1 cm in diameter. In all cases, mice were anesthetized with 1–2% isoflurane (with room air) for administration of radiopharmaceuticals.

PET tracers

^{18}F-FMISO and ^{18}F-FDG were prepared according to published methods (15) with an automated modular-lab (Sumitomo Heavy Industry, Japan). In brief, ^{18}F-fluoride was passed through a QMA cartridge and introduced into the reactor according to the principle of ion exchange by using $K_2CO_3/K222$ mixture. Anhydrous acetonitrile (0.5 mL) was introduced into the reaction vessel and heated with the help of a nitrogen flow until sufficiently dry (azeotropy). For the synthesis of ^{18}F-FMISO, 1.5 mL of acetonitrile containing 10 mg of the precursor NITTP [1-(2'-nitro-1'-imidazolyl)-2-O-tetrahydropyranyl-3-O-toluenesulfonyl-propanediol] (ABX) was added and heated at 110 °C for 6 min, followed by hydrolysis with 1 M HCl (0.75 mL) at 100 °C for 3 min. After cooling to room temperature, a neutralizing solution (3 M sodium acetate, 0.75 mL) was introduced and then

transferred to semi-preparative C-18 high performance liquid chromatography (HPLC) for purification. For preparation of ^{18}F-FDG, all procedures were similar except that 20 mg of mannose triflate (ABX) and purification columns (IC-H, PS-2, Al-N) was used as precursor and to remove impurities, respectively. Radiochemical yields and radiochemical purities for ^{18}F-FMISO and ^{18}F-FDG were determined by thin-layer chromatography and HPLC, respectively.

Micro PET imaging

As described previously, all animals (n=6) were secured in supine position, and imaged using a Siemens Inveon micro PET system which was equipped with Inveon data acquisition workplace and ASI Pro VM software for preparing sinograms and image reconstruction. Energy and coincidence timing window was set to 350–650 keV. Images were reconstructed using a 3-dimensional ordered subset expectation maximization (3D-OSEM) algorithm with 0.78 mm thickness, 128×128 matrix. Regions of interests (ROI) were placed on the tumors and muscle tissues. The average radioactivity concentration was obtained from the average pixel values within the multiple ROI volume using PMOD analysis software for data analysis.

The established breast tumor bearing mice were randomly divided into two groups. Mice in ^{18}F-FMISO group (n=3) were injected via the tail vein with ^{18}F-FMISO (approximately 3.7 MBq) without anesthesia. Two hours after tracer injection, animals were anesthetized by i.p. injection of sodium pentobarbital at a dose of 45.0 mg/kg. PET acquisition time was fixed to 10 min for PET scans. For mice in ^{18}F-FDG group (n=3), all procedures were similar except that the mice were made to fast for 12 hours before ^{18}F-FDG injection and PET scans were performed 1 hour after tracer injection to compare with ^{18}F-FMISO PET imaging.

Immunohistochemical staining

The hypoxia marker, pimonidazole hydrochloride (1-[(2-hydroxy-3-piperidinyl)propyl]-2-nitroimidazole hydrochloride) was dissolved in physiological saline at a concentration of 20 mg/mL. The proliferation marker, bromodeoxyuridine was first dissolved in dimethyl sulfoxide and further diluted in physiological saline to a final concentration of 20 mg/mL. A mixture of pimonidazole (2 mg) and bromodeoxyuridine (4 mg) was injected via the tail vein, along with the injection of PET tracers. In all cases, fresh drug solutions were prepared on the day of injection.

Immediately after animal sacrifice, MDA-MB-231 tumor samples from both ^{18}F-FMISO and ^{18}F-FDG groups were quickly removed, frozen in OCT medium (Tissue-Tek; Sakura Finetek, USA) and cut with a cryotome (Shandon FSE; Thermo, UK) into 10 micrometer sections and were adhered to poly-L-lysine-coated glass microscope slides.

Sections were mounted on slides containing DAPI to visualize nuclei. Pimonidazole and bromodeoxyuridine were obtained after DAPI. In order to minimize issues associated with section alignment and registration, the same tumor section or contiguous adjacent sections were used for all images. Briefly, slides were air dried, fixed in cold acetone (4 °C) for 20 min, and incubated with SuperBlock (37515, Pierce Biotechnology, Rockford, IL, USA) at room temperature for 30 min. All antibodies were also applied in SuperBlock. Sections were then incubated with FITC conjugated anti-pimonidazole monoclonal antibody (Hypoxyprobe Inc., Burlington, MA, USA), diluted 1:50, for 1 hour at room temperature. For bromodeoxyuridine staining, adjacent sections to those used for pimonidazole were treated with 2N HCl for 10 min at room temperature followed by 0.1 M Borax for 10 min at room temperature. Sections were then exposed to Alexa Fluor594-conjugated anti-bromodeoxyuridine antibody (1:50 dilution, Molecular Probes, Eugene, OR, USA) for 1 hour at room temperature (16,17).

Fluorescence micrographs of these slides were taken from an inverted fluorescence microscope (AXIO Vert.A1; Zeiss, Germany) with magnification at ×100. Pimonidazole was imaged using green filter. Bromodeoxyuridine was imaged using a red filter. H&E was imaged by light microscopy.

Results

Preparation of ^{18}F-FMISO and ^{18}F-FDG

^{18}F-FMISO and ^{18}F-FDG were prepared easily and efficiently using an automated synthesizer. The results were obtained by Rf values from TLC which labeling yield was over 99%.

Micro PET imaging

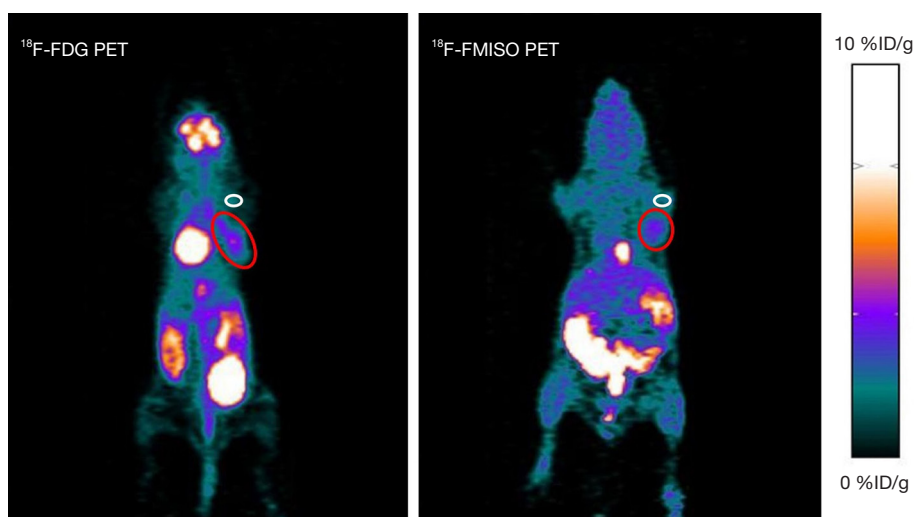All mice survived anesthesia, tumor implantation and

Figure 1 Representative PET coronal slices of ¹⁸F-FMISO and ¹⁸F-FDG in MDA-MB-231 nude mice. High radioactivity accumulations were found in tumors. ¹⁸F-FDG showed physiologically high uptake in brain, heart, bladder and intestinal tracts. For ¹⁸F-FMISO, intestines and liver as well as bladder could be seen in highlighted area. ROI of tumor (red circle) and ROI of muscle (white circle) were shown. Scale bar for both of ¹⁸F-FMISO and ¹⁸F-FDG PET imaging is as indicated.

imaging experiments. MDA-MB-231 cells were inoculated into right forelimb of nude mice. Results of histological examinations indicated the tumor cells of xenografts have intact nucleus and cytoplasm.

The small animal PET imaging studies for the biodistribution of ¹⁸F-FMISO and ¹⁸F-FDG were done in the MDA-MB-231 TNBC models at different time points, which is 60 min p.i. for ¹⁸F-FDG and 90 min p.i. for ¹⁸F-FMISO. *Figure 1* illustrates the representative PET images of tumor-bearing mice injected with approximately 3.7 MBq radiotracers. The images of ¹⁸F-FDG and ¹⁸F-FMISO showed a similar trend with the biodistribution data (15,18). Tumors were visualized with clear contrast by red circles. For ¹⁸F-FMISO, intestines and liver as well as bladder could be seen in highlighted area. ¹⁸F-FDG showed physiologically high uptake in brain, heart, bladder and intestinal tracts as seen in *Figure 1*. The quantitative radioactivity of ¹⁸F-FMISO and ¹⁸F-FDG in tumor were 2.18±0.15 and 3.84±0.54 %ID/g, respectively. The quantitative radioactivity of ¹⁸F-FMISO and ¹⁸F-FDG in muscle were 1.23±0.08 and 0.59±0.09 %ID/g, respectively. The tumor-to-muscle ratios were 1.79±0.015 and 7.11±2.84 for ¹⁸F-FMISO and ¹⁸F-FDG, respectively (*Figure 2*).

Immunohistochemical staining (Figure 3)

Representative examples pimonidazole binding and proliferation are shown in MDA-MB-231 subcutaneous xenografts for both ¹⁸F-FMISO and ¹⁸F-FDG groups (*Figure 3B*). Cancer cells were further divided into two subcategories according to oxygenation status and cellular proliferation: cancer cells close to functional blood vessels (positive DAPI) stained negatively for pimonidazole but positively for bromodeoxyuridine, indicating that the cells were well oxygenated and proliferative. Cancer cells away from functional blood vessels stained positively for pimonidazole but negatively for bromodeoxyuridine, indicating that these cancer cells were hypoxic and less proliferative.

Conclusions

Breast cancer is the most frequently diagnosed cancer and a major cause of death in women worldwide (19). Over 90% of all breast cancer deaths are the result of metastasis, primarily to the bone, lung, liver, brain and lymph nodes (20). Metastases are found in only 6% of women with breast cancer at the time of initial presentation, yet 30% of women with early stage disease at diagnosis will eventually progress to metastatic disease (21). Cancers that lack expression of ER, PR, or HER2 are designated "triple negative" and, in the absence of any targeted therapy, are treated with cytotoxic chemotherapy, with greatly increased rates of relapse, metastasis, and death compared to the other breast cancer
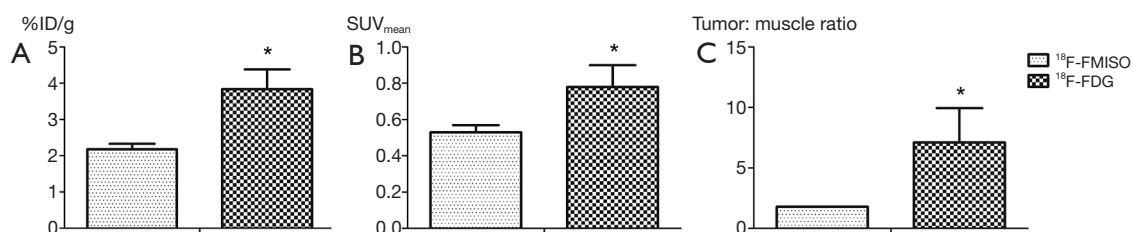
Figure 2 ^{18}F-FMISO uptake and ^{18}F-FDG uptake in MDA-MB-231 tumor tissue by analyzing micro PET images. (A,B) ^{18}F-FMISO uptake and ^{18}F-FDG uptake in MDA-MB-231 tumor tissue; (C) tumor/muscle radio of ^{18}F-FMISO and ^{18}F-FDG in MDA-MB-231 nude mice model. *, P<0.05 compared with ^{18}F-FDG group.
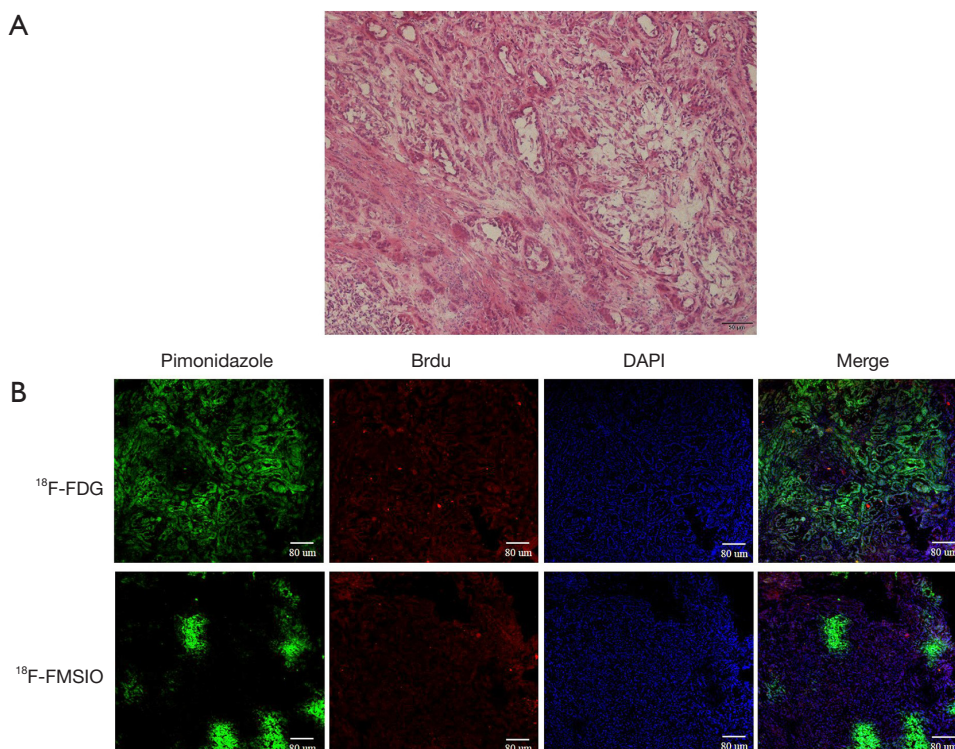

Figure 3 Findings of immunohistochemical staining. (A) Microscopic histological examination of frozen tumor section stained by hematoxylin and eosin. Scale bar is as indicated; (B) complex microenvironment of MDA-MB-231 subcutaneous xenografts from both groups. Immunofluorescent images from MDA-MB-231 cryosections show hypoxia and proliferation. Pimonidazole is shown as green, Brdu as red, and DAPI as blue. Scale bar is as indicated.

types. In this study, we successfully evaluated the hypoxic microenvironment of the triple negative breast cancer with PET tracer ^{18}F-FMISO.

In this study, we have shown that the microenvironment of MDA-MB-231 xenografts is complex and highly heterogeneous, being composed of viable, proliferative, and hypoxic cancer cells; nonhypoxic and highly proliferative cancer cells (*Figure 3A*). This finding is consistent with histologic findings in triple-negative breast cancer

patients (22), suggesting that our tumor models can mimic human breast cancer. Because of the complex tumor microenvironment, it is impossible to generate identical experimental xenografts for the purpose of detecting hypoxia with ^{18}F-FMISO.

Hypoxic tumors accumulate and propagate cancer stem cells (CSC). Hypoxia reduces the effectiveness of radiotherapy, increases metastasis risk and reduces the effectiveness of surgery. What's more, hypoxic tumors are resistant

to the effects of chemotherapy and chemoradiation (1). On the other hand, the presence of severe hypoxia may have its advantage as a specific target for molecular imaging of cancer, which may be difficult to detect with current anatomic imaging modalities like CT and/or MRI (23,24).

High uptakes of ^{18}F-FMISO were observed in kidney, bladder, liver and guts. These findings are in good agreement with the fact that ^{18}F-FMISO is a relatively lipophilic molecule (partition coefficient =0.40, log P=−0.40) (25). The mean total excretion of ^{18}F-FMISO in human urine is as low as 3% of the total injected dose (25,26), but metabolites of ^{18}F-FMISO are typically excreted into the urine (83% intact at 95 min post injection). It was also reported that large amount of anaerobic bacteria present in the large intestine may result in high intestinal uptake of ^{18}F-FMISO (18). We have successfully compared ^{18}F-FDG and ^{18}F-FMISO uptake by conducting serials micro-PET scans on the same MDA-MB-231 xenograft models (*Figure 1*). Highest accumulation of ^{18}F-FDG was found in bladder as seen in *Figure 1* demonstrating that the primary clearance mode of ^{18}F-FDG was the renal-urinary excretion pathway. High radioactivity of both ^{18}F-FMISO and ^{18}F-FDG in tumor xenografts were observed (2.18±0.15 and 3.84±0.54 %ID/g, respectively). The quantitative radioactivity of ^{18}F-FMISO and ^{18}F-FDG in muscle were 1.23±0.08 and 0.59± 0.09 %ID/g, respectively. The tumor-to-muscle ratios were 1.79±0.015 and 7.11±2.84 for ^{18}F-FMISO and ^{18}F-FDG, respectively (*Figure 2*). These results indicate that not only ^{18}F-FDG accumulates in metastatic triple-negative MDA-MB-231 human breast cancer xenografts, but also ^{18}F-FMISO. As it is known that the ^{18}F-FMISO PET regions of interest with tumor-to-background (T:B) ratios of 1.3 and above are often demarcated as hypoxic (27), with the results of immunohistochemical staining we can conclude ^{18}F-FMISO could illustrate the status of hypoxic microenvironment in this model. It is reported that tumor oxygenation at pO_2 levels of 10 mmHg or over would not be detected by ^{18}F-FMISO PET scans (28). A preliminary study of the reproducibility of ^{18}F-FMISO PET imaging revealed a considerable variability in scans performed 3 days apart in the same patient (29). Further research would be necessary.

Although acute hypoxia results in accelerated glycolysis as well as cellular metabolism are slowed in chronic hypoxia, hypoxia and glucose metabolism, as reflected by ^{18}F-FMISO and ^{18}F-FDG PET imaging, respectively, may not follow a simple relationship. Glucose metabolism is affected by many processes beside hypoxia. For example, cellular proliferation will result in accelerated glucose metabolism in the absence of hypoxia. Moreover, the poor blood supply that causes hypoxia might lead to significantly reduced delivery of nutrients such as glucose in chronic situations and hence decreased glucose uptake. The discordance between ^{18}F-FMISO and ^{18}F-FDG might also be a reflection of vascularization and blood supply (30). Approximately 25–40% of all invasive breast cancers contain hypoxic regions (31). Two main types of tumour hypoxia have been described: chronic and acute (32). Chronic (diffusion-limited) hypoxia is defined as cells exposed to low-oxygen levels for longer than 24 hours, which frequently occurs in poorly vascularized regions. Acute (perfusion-limited) hypoxia involves transient exposure of cells to hypoxia, ranging from minutes up to 24 hours. This typically involves cells located near capillaries exhibiting transitory interruptions in blood flow (e.g., as a result of functional changes in vascular stability).

In the current study, we used correlative imaging methodologies to examine the uptake of ^{18}F-FMISO in microscopic triple-negative MDA-MB-231 tumor and relate this to hypoxia and perfusion (*Figure 3B*). ^{18}F-FMISO uptake, visualized by Micro-PET, was compared with immunofluorescent visualization of pimonidazole and bromodeoxyuridine binding. We found that high ^{18}F-FMISO uptake was closely associated with pimonidazole-positive TNBC tumor. ^{18}F-FMISO in PET may noninvasively detect hypoxic status in TNBC cells at macroscopic level.

Over expression of hypoxia-inducible factor-1 alpha (HIF-1α) is clearly clinically relevant to survivability of breast cancer. It has now been shown that increased expression of HIF-1α is highly correlated with increased mortality and metastasis (33-37). However, we didn't assess the relationships among HIF-1α, ^{18}F-FMISO uptake and ^{18}F-FDG uptake in this TNBC model. We will evaluate the relationships in our next study. Besides, there were several limitations to our study. Our lack of negative control (TNBC tumor without hypoxia), small group size and no immunohistochemical quantitative analysis within the study limits the ability to generalize our findings. Despite these limitations, our data adds to the knowledge of hypoxia microenvironment of TNBC.

Acknowledgments

Footnote

Conflicts of Interest: All authors have completed the ICMJE uniform disclosure form (available at http://dx.doi.org/10.21037/tcr.2016.06.07). The authors have no conflicts of interest to declare.

Ethical Statement: The authors are accountable for all aspects of the work in ensuring that questions related to the accuracy or integrity of any part of the work are appropriately investigated and resolved. All animal experimental protocols were conducted in compliance with the Guidelines for the care and use of research animals established by the Animals Affairs Committee of Sichuan Cancer Hospital (permit number: 20150194).

Open Access Statement: This is an Open Access article distributed in accordance with the Creative Commons Attribution-NonCommercial-NoDerivs 4.0 International License (CC BY-NC-ND 4.0), which permits the non-commercial replication and distribution of the article with the strict proviso that no changes or edits are made and the original work is properly cited (including links to both the formal publication through the relevant DOI and the license). See: https://creativecommons.org/licenses/by-nc-nd/4.0/.

References

1. Walsh JC, Lebedev A, Aten E, et al. The clinical importance of assessing tumor hypoxia: relationship of tumor hypoxia to prognosis and therapeutic opportunities. Antioxid Redox Signal 2014;21:1516-54.

2. Pires IM, Olcina MM, Anbalagan S, et al. Targeting radiation-resistant hypoxic tumour cells through ATR inhibition. Br J Cancer 2012;107:291-9.

3. Höckel M, Knoop C, Schlenger K, et al. Intratumoral pO2 histography as predictive assay in advanced cancer of the uterine cervix. Adv Exp Med Biol 1994;345:445-50.

4. Brizel DM, Scully SP, Harrelson JM, et al. Tumor oxygenation predicts for the likelihood of distant metastases in human soft tissue sarcoma. Cancer Res 1996;56:941-3.

5. Yu B, Baumgärtl H, Lübbers DW. An improved polarographic multiwire surface PO2 electrode, particularly for measurement of high PO2 values. Adv Exp Med Biol 1984;169:877-86.

6. Lee ST, Scott AM. Hypoxia positron emission tomography imaging with 18f-fluoromisonidazole. Semin Nucl Med 2007;37:451-61.

7. Bentzen L, Keiding S, Nordsmark M, et al. Tumour oxygenation assessed by 18F-fluoromisonidazole PET and polarographic needle electrodes in human soft tissue tumours. Radiother Oncol 2003;67:339-44.

8. Komar G, Seppänen M, Eskola O, et al. 18F-EF5: a new PET tracer for imaging hypoxia in head and neck cancer. J Nucl Med 2008;49:1944-51.

9. Ziemer LS, Evans SM, Kachur AV, et al. Noninvasive imaging of tumor hypoxia in rats using the 2-nitroimidazole 18F-EF5. Eur J Nucl Med Mol Imaging 2003;30:259-66.

10. Postema EJ, McEwan AJ, Riauka TA, et al. Initial results of hypoxia imaging using 1-alpha-D: -(5-deoxy-5-[18F]-fluoroarabinofuranosyl)-2-nitroimidazole (18F-FAZA). Eur J Nucl Med Mol Imaging 2009;36:1565-73.

11. Beck R, Röper B, Carlsen JM, et al. Pretreatment 18F-FAZA PET predicts success of hypoxia-directed radiochemotherapy using tirapazamine. J Nucl Med 2007;48:973-80.

12. Yuan H, Schroeder T, Bowsher JE, et al. Intertumoral differences in hypoxia selectivity of the PET imaging agent 64Cu(II)-diacetyl-bis(N4-methylthiosemicarbazone). J Nucl Med 2006;47:989-98.

13. Lewis JS, Laforest R, Dehdashti F, et al. An imaging comparison of 64Cu-ATSM and 60Cu-ATSM in cancer of the uterine cervix. J Nucl Med 2008;49:1177-82.

14. Zimny M, Gagel B, DiMartino E, et al. FDG--a marker of tumour hypoxia? A comparison with [18F] fluoromisonidazole and pO2-polarography in metastatic head and neck cancer. Eur J Nucl Med Mol Imaging 2006;33:1426-31.

15. Huang T, Civelek AC, Li J, et al. Tumor microenvironment-dependent 18F-FDG, 18F-fluorothymidine, and 18F-misonidazole uptake: a pilot study in mouse models of human non-small cell lung cancer. J Nucl Med 2012;53:1262-8.

16. Li XF, Sun X, Ma Y, et al. Detection of hypoxia in microscopic tumors using 131I-labeled iodo-azomycin galactopyranoside (131I-IAZGP) digital autoradiography.

Eur J Nucl Med Mol Imaging 2010;37:339-48.

17. Li XF, Ma Y, Sun X, et al. High 18F-FDG uptake in microscopic peritoneal tumors requires physiologic hypoxia. J Nucl Med 2010;51:632-8.

18. Liu RS, Chou TK, Chang CH, et al. Biodistribution, pharmacokinetics and PET imaging of [(18)F] FMISO, [(18)F]FDG and [(18)F]FAc in a sarcoma- and inflammation-bearing mouse model. Nucl Med Biol 2009;36:305-12.

19. Jemal A, Bray F, Center MM, et al. Global cancer statistics. CA Cancer J Clin 2011;61:69-90.

20. Libreros S, Garcia-Areas R, Shibata Y, et al. Induction of proinflammatory mediators by CHI3L1 is reduced by chitin treatment: decreased tumor metastasis in a breast cancer model. Int J Cancer 2012;131:377-86.

21. O'Shaughnessy J. Extending survival with chemotherapy in metastatic breast cancer. Oncologist 2005;10 Suppl 3:20-9.

22. Montagna E, Maisonneuve P, Rotmensz N, et al. Heterogeneity of triple-negative breast cancer: histologic subtyping to inform the outcome. Clin Breast Cancer 2013;13:31-9.

23. Gillies RJ, Raghunand N, Karczmar GS, et al. MRI of the tumor microenvironment. J Magn Reson Imaging 2002;16:430-50.

24. Dallaudiere B, Hummel V, Hess A, et al. Tumoral hypoxia in osteosarcoma in rats: preliminary study of blood oxygenation level-dependent functional MRI and 18F-misonidazole PET/CT with diffusion-weighted MRI correlation. AJR Am J Roentgenol 2013;200:W187-92.

25. Graham MM, Peterson LM, Link JM, et al. Fluorine-18-fluoromisonidazole radiation dosimetry in imaging studies. J Nucl Med 1997;38:1631-6.

26. Bruehlmeier M, Roelcke U, Schubiger PA, et al. Assessment of hypoxia and perfusion in human brain tumors using PET with 18F-fluoromisonidazole and 15O-H2O. J Nucl Med 2004;45:1851-9.

27. Koh WJ, Rasey JS, Evans ML, et al. Imaging of hypoxia in human tumors with [F-18]fluoromisonidazole. Int J Radiat Oncol Biol Phys 1992;22:199-212.

28. Cárdenas-Navia LI, Mace D, Richardson RA, et al. The pervasive presence of fluctuating oxygenation in tumors. Cancer Res 2008;68:5812-9.

29. Nehmeh SA, Lee NY, Schröder H, et al. Reproducibility of intratumor distribution of (18)F-fluoromisonidazole in head and neck cancer. Int J Radiat Oncol Biol Phys 2008;70:235-42.

30. Rajendran JG, Mankoff DA, O'Sullivan F, et al. Hypoxia and glucose metabolism in malignant tumors: evaluation by [18F]fluoromisonidazole and [18F]fluorodeoxyglucose positron emission tomography imaging. Clin Cancer Res 2004;10:2245-52.

31. Lundgren K, Holm C, Landberg G. Hypoxia and breast cancer: prognostic and therapeutic implications. Cell Mol Life Sci 2007;64:3233-47.

32. Kalliomäki TM, McCallum G, Wells PG, et al. Progression and metastasis in a transgenic mouse breast cancer model: effects of exposure to in vivo hypoxia. Cancer Lett 2009;282:98-108.

33. Bos R, van Diest PJ, van der Groep P, et al. Expression of hypoxia-inducible factor-1alpha and cell cycle proteins in invasive breast cancer are estrogen receptor related. Breast Cancer Res 2004;6:R450-9.

34. Currie MJ, Hanrahan V, Gunningham SP, et al. Expression of vascular endothelial growth factor D is associated with hypoxia inducible factor (HIF-1alpha) and the HIF-1alpha target gene DEC1, but not lymph node metastasis in primary human breast carcinomas. J Clin Pathol 2004;57:829-34.

35. Dales JP, Garcia S, Meunier-Carpentier S, et al. Overexpression of hypoxia-inducible factor HIF-1alpha predicts early relapse in breast cancer: retrospective study in a series of 745 patients. Int J Cancer 2005;116:734-9.

36. Gruber G, Greiner RH, Hlushchuk R, et al. Hypoxia-inducible factor 1 alpha in high-risk breast cancer: an independent prognostic parameter? Breast Cancer Res 2004;6:R191-8.

37. Schindl M, Schoppmann SF, Samonigg H, et al. Overexpression of hypoxia-inducible factor 1alpha is associated with an unfavorable prognosis in lymph node-positive breast cancer. Clin Cancer Res 2002;8:1831-7.